Differential distribution of endoplasmic reticulum controls metabotropic signaling and plasticity at hippocampal synapses

Niklaus Holbro, Åsa Grunditz, and Thomas G. Oertner[1]

Friedrich Miescher Institute for Biomedical Research, Maulbeerstrasse 66, CH-4058 Basel, Switzerland

Edited by Roger A. Nicoll, University of California, San Francisco, CA, and approved July 22, 2009 (received for review May 8, 2009)

Synaptic plasticity is considered essential for learning and storage of new memories. Whether all synapses on a given neuron have the same ability to express long-term plasticity is not well understood. Synaptic microanatomy could affect the function of local signaling cascades and thus differentially regulate the potential for plasticity at individual synapses. Here, we investigate how the presence of endoplasmic reticulum (ER) in dendritic spines of CA1 pyramidal neurons affects postsynaptic signaling. We show that the ER is targeted selectively to large spines containing strong synapses. In ER-containing spines, we frequently observed synaptically triggered calcium release events of very large amplitudes. Low-frequency stimulation of these spines induced a permanent depression of synaptic potency that was independent of NMDA receptor activation and specific to the stimulated synapses. In contrast, no functional changes were induced in the majority of spines lacking ER. Both calcium release events and long-term depression depended on the activation of metabotropic glutamate receptors and inositol trisphosphate receptors. In summary, spine microanatomy is a reliable indicator for the presence of specific signaling cascades that govern plasticity on a micrometer scale.

long-term depression | metabotropic glutamate receptor | metaplasticity | spine apparatus | dendritic spines

Activity-dependent changes in synaptic strength are thought to be essential for learning and the formation of new memories (1). The intracellular signaling cascades underlying different forms of synaptic plasticity have been studied extensively at the CA3 to CA1 projection in the hippocampus. Although long-term potentiation at these synapses is strictly NMDA receptor-dependent, at least two mechanistically distinct forms of long-term depression (LTD) have been described, triggered by the activation of NMDA receptors (NMDARs) and metabotropic glutamate receptors (mGluRs), respectively (2). Although the potential for NMDAR-dependent plasticity can be regulated by the subunit composition of the receptor itself, much less is known about the regulation of mGluR-dependent plasticity (3). Aberrant mGluR signaling and dysregulated synaptic plasticity have been implicated in severe mental disorders, such as fragile X mental retardation (4). The induction of mGluR-dependent LTD is known to involve activation of postsynaptic group I mGluRs and inositol trisphosphate (IP_3)-mediated calcium release from the endoplasmic reticulum (ER) (reviewed in ref. 5). Interestingly, only a small subset of dendritic spines on CA1 pyramidal cells contains ER (6). The heterogeneous distribution of this organelle very well could affect the plasticity of individual synapses (7, 8).

In all previous studies of synaptic depression, plasticity was induced at large numbers of synapses simultaneously. However, this strategy does not allow the investigation of functional differences between individual synaptic connections. Differences in synaptic microanatomy, such as the presence of specialized organelles, could strongly regulate plasticity on a local scale, resulting in functional heterogeneities between individual contacts. To test this hypothesis, we compared postsynaptic signaling in synapses made on spines containing ER and spines without ER. To stimulate identified synapses in intact tissue, we combined two-photon imaging with two-photon glutamate uncaging. We show that ER is specifically associated with potent synapses and governs the potential for mGluR-mediated synaptic depression. In spines containing ER, calcium influx through NMDARs was dwarfed by large calcium release events that are likely to play a key role in plasticity induction. The preferential association of ER with the most potent synapses suggests that mGluR-mediated depression plays an important role in the balance of excitation, counteracting the tendency of potent synapses to become even stronger over time.

Results

Genetic Approach To Identify ER-Containing Spines in CA1 Pyramidal Cells. To visualize the ER in intact hippocampal tissue, we constructed a green ER label by fusing EGFP with ER-targeting and ER-retention sequences (9). Organotypic hippocampal slice cultures were cotransfected biolistically with the ER label and a cytoplasmic red fluorescent protein (RFP) to visualize cell morphology (Fig. 1*A*). Two-photon microscopy was used to image transfected CA1 pyramidal cells at high resolution and identify ER-containing (ER+) and other (ER−) spines on oblique dendrites close to the soma (Fig. 1*B*). Spines were considered ER+ if they had a clear GFP signal inside the head (Fig. 1*C*); spines with traces of ER in the neck region were not analyzed. Analysis of several transfected CA1 pyramidal cells showed that 18.7 ± 2.3% of spines were positive for the ER label (n = 318 spines, 8 cells). A similar fraction of ER-containing spines has been reported in acute slices by using electron microscopic reconstruction of CA1 cell dendrites (6). To test whether spine ER was continuous with dendritic ER, we performed fluorescence recovery after photobleaching (FRAP) experiments on the ER label. A brief laser pulse (930 nm) was used to bleach the green ER label inside the spines (Fig. 1*D*). On average, ER fluorescence recovered with a time constant of 210 ± 39 ms (n = 33 spines). These data indicate that dendritic spines contain ER structures that are connected to dendritic ER and that ER constituents (such as ions and proteins) can rapidly diffuse inside the ER lumen from the spine to the dendrite and vice versa.

ER-Containing Spines Have Large Heads and Often Contain a Spine Apparatus. Quantification of spine morphology showed that ER+ spines had significantly larger cytoplasmic volumes (0.058 ± 0.005 μm^3, n = 49) than the rest of the population

Author contributions: N.H. and T.G.O. designed research; N.H. and Å.G. performed research; N.H. analyzed data; and N.H. and T.G.O. wrote the paper.

The authors declare no conflict of interest.

This article is a PNAS Direct Submission.

[1]To whom correspondence should be addressed. E-mail: thomas.oertner@fmi.ch .

This article contains supporting information online at www.pnas.org/cgi/content/full/0905110106/DCSupplemental.

NEUROSCIENCE

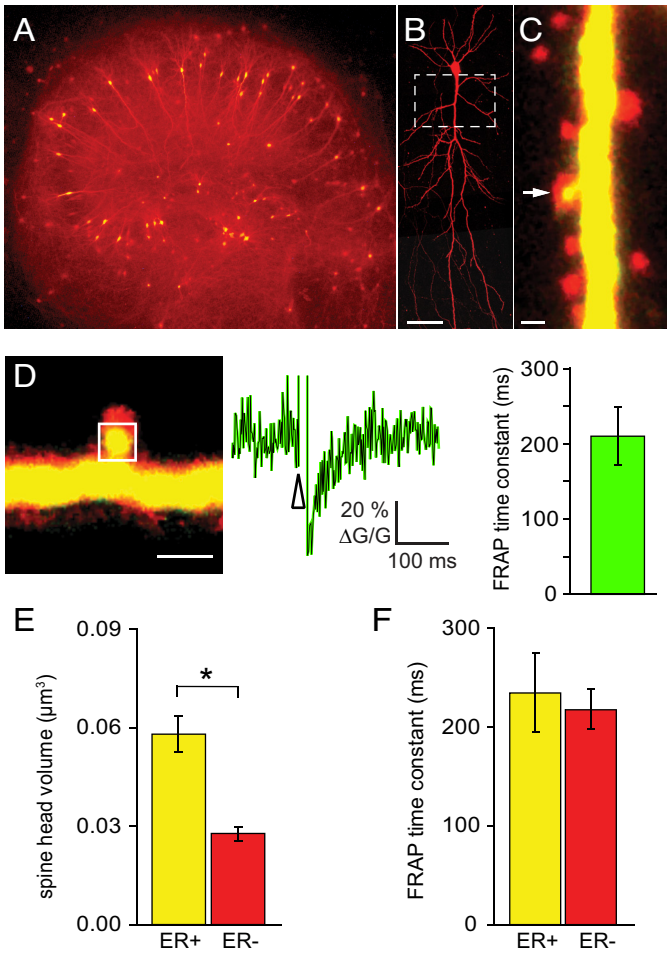

Fig. 1. ER labeling and spine properties. (*A*) Organotypic hippocampal cultures were transfected biolistically with a cytoplasmic RFP (red) and an ER-targeted EGFP (GFP-ER, green). (*B*) Two-photon image (maximum intensity projection) of transfected CA1 pyramidal cell. White box indicates region of analyzed oblique dendrites. (Scale bar: 50 μm.) (*C*) Dendrite of a transfected CA1 pyramidal cell with one large ER-containing spine (arrow). Overlay of red (RFP) and green (GFP-ER) fluorescence results in yellow color. (Scale bar: 1 μm.) (*D*) FRAP of the GFP-ER label was performed on ER+ spines, and GFP diffusion inside the ER lumen was monitored (n = 33 spines). (*E*) Spine head volume of ER+ spines was significantly larger compared with that of ER− spines (ER+, n = 49; ER−, n = 91) (*F*) Cytoplasmic FRAP time constants were not different in ER+ and ER− spines (ER+, n = 26; ER−, n = 35). Values in *D–F* represent mean ± SEM.

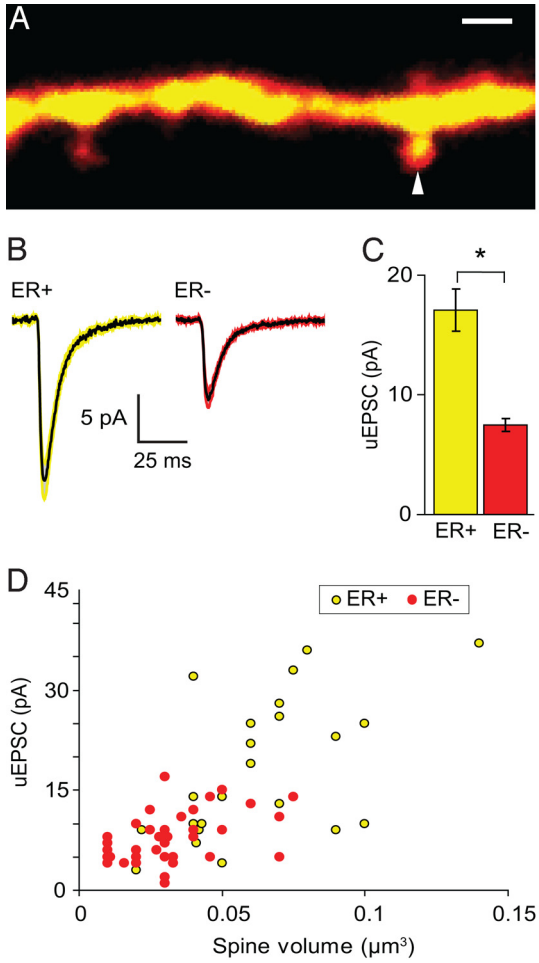

Fig. 2. ER-containing spines bear strong synapses. (*A*) Stimulation of ER-containing spine by two-photon glutamate uncaging (arrowhead). (Scale bar: 1 μm.) (*B*) Average uEPSCs for ER-containing (n = 30) and other spines (n = 44). Colored region represents SEM. (*C*) Peak amplitude of uEPSC was significantly larger in ER+ spines (n = 30) compared with that in ER− spines (n = 44). Values in *C* represent mean ± SEM. (*D*) Relationship between spine volume and uEPSC amplitude (n = 62).

(0.028 ± 0.002 μm^3, n = 91; Fig. 1*E*). Spine heads are separated from their parent dendrite by a thin spine neck, allowing biochemical compartmentalization of second messengers (10). The ER could affect the diffusional coupling between spine head and parent dendrite by physically obstructing the neck. To address this issue, we measured FRAP time constants (τ) of cytoplasmic RFP in ER-containing and other spines. We bleached ≈30% of the cytoplasmic red fluorescence inside the spine and monitored fluorescence recovery. The recovery time constants in the two groups of spines were not significantly different (τ_{ER+} = 235 ± 40 ms, n = 26; τ_{ER-} = 218 ± 20 ms, n = 35; Fig. 1*F*), demonstrating that the ER did not block cytoplasmic diffusion between spine head and dendrite. In fact, because of the larger head volumes of ER+ spines, these would be expected to have longer time constants, assuming identical neck properties (11, 12). The similar time constants therefore suggest that the necks of ER+ spines provided an even weaker diffusional barrier compared with those of spines lacking ER.

In spines of pyramidal cells, ER often forms a specialized organelle consisting of stacked membrane discs, the spine apparatus (6). To assess which fraction of ER+ spines in our sample contained this organelle, we combined live ER imaging with posthoc immunohistochemistry against synaptopodin, a protein associated with the spine apparatus (13) (Fig. S1*A*). We found that the majority (78%) of ER+ spines were also positive for synaptopodin (Fig. S1*B*) and thus very likely contained a spine apparatus.

Synapses on ER-Containing Spines Have a High Potency. To assess the functional properties of spine synapses, we stimulated individual spines by two-photon glutamate uncaging. First, we identified ER+ spines on oblique dendrites (Fig. 2*A*). After spine preselection, cells were patch-clamped, and glutamate was uncaged on identified spines. On average, uncaging-evoked excitatory postsynaptic currents (uEPSCs) had amplitudes of 11.4 ± 0.7 pA (n = 74 spines, 23 cells), similar to the amplitudes of miniature EPSCs in these cells (12.4 ± 0.6 pA, n = 8 cells). Stimulation of ER+ spines evoked significantly larger uEPSCs (17.1 ± 1.9 pA, n = 30) than stimulation of other spines (7.5 ± 0.5 pA, n = 44; Fig. 2 *B* and *C*). To exclude systematic differences in stimulation intensity, we consistently stimulated one to two ER+ and control

spines on the same dendrite (distance <25 μm). Furthermore, we compared the amount of bleaching of a cytoplasmic red dye by the uncaging laser pulse (calibration method used in ref. 14), which was identical in ER-containing and other spines (Fig. S2). This control verified that both groups of spines were stimulated with the same local laser intensity. In our sample of spine synapses, uEPSC amplitude was positively correlated with spine volume ($R^2 = 0.46, n = 62$; Fig. 2*D*), which is in line with previous studies (15, 16). Thus, our data indicate that high-potency synapses are located on large spines and these high-potency synapses are often associated with spine ER. We would like to point out that no causal relationship should be inferred from these correlations between morphology and function.

Similar NMDAR-Mediated Calcium Transients in ER+ and ER− Spines. The ER potentially could modulate the time course of postsynaptic calcium transients, which are an important trigger for synaptic plasticity (17, 18). To compare calcium transients in spines with and without ER, we filled transfected CA1 pyramidal cells with a mixture of a green calcium-sensitive dye (Fluo5F) and a red calcium-insensitive dye (Alexa Fluor 594). At the excitation wavelength and laser power used in the calcium imaging experiments (810 nm, ≈10 mW), GFP and RFP fluorescence was negligible. Glutamate uncaging evoked spine calcium transients (CaTs) with short latencies (Fig. 3*A*). The amplitudes of these rapid CaTs have been shown to mainly depend on the activation of different subtypes of NMDARs and other voltage-sensitive channels (19–21). Consistent with these reports, we found that the NMDAR antagonist D-4-[(2E)-3-Phosphono-2-propenyl]-2-piperazinecarboxylic acid (dCPP) (10 μM) strongly reduced peak amplitude (22.8% of control amplitude, $n = 4$). Peak amplitudes of short-latency CaTs (Fig. 3*B*) were not significantly different between ER-containing spines ($\Delta G/R = 26 \pm 6\%, n = 19$) and other spines ($\Delta G/R = 19 \pm 3\%, n = 26$). The decay time constants (τ_{decay}) were also very similar (ER+ $\tau_{decay} = 164 \pm 19$ ms; ER− $\tau_{decay} = 179 \pm 34$ ms). Depletion of intracellular calcium stores with thapsigargin (10 μM) did not reduce peak amplitude of these rapid calcium transients (116% of control amplitude, $n = 9$ ER+ spines), suggesting that calcium release did not significantly boost NMDAR-mediated signals. Our data therefore indicate that spine ER is not a major modulator of NMDAR- mediated CaTs during synaptic activity.

mGluR-Dependent Calcium Release in ER-Containing Spines. As described above, glutamate uncaging triggered fast rising calcium transients (average time to peak, 47 ms) with a slow decay ($\tau_{decay} = 173 \pm 21$ ms) in all spines tested. In addition, in some spines, we observed a second, delayed rise in calcium concentration (average delay, 470 ± 41 ms; Fig. 3*C*). This second calcium transient (CaT2) reached much higher amplitudes than the fast, NMDAR-mediated transient (CaT1, $\Delta G/R = 26 \pm 6\%$; CaT2, $\Delta G/R = 141 \pm 26\%$; Fig. 3*D*). Delayed CaTs were observed in seven of 19 ER+ spines but never in ER− spines ($n = 26$). Our best estimate for the frequency of spines with delayed CaTs is 7/19 = 0.37, so assuming a binomial distribution, the probability of observing no delayed CaTs in ER− spines is 6.6×10^{-6}. Therefore, ER+ and ER− spines represent two distinct populations with respect to their calcium signaling.

Delayed CaTs never preceded uncaging stimulation but appeared to be triggered by the stimulation in a stochastic fashion (Fig. 3*C*). In the spines that showed delayed CaTs, they occurred in ≈20% of the individual stimulations (range 6–43%). Simultaneous voltage-clamp recordings revealed no somatic depolarization during delayed CaTs, making voltage-gated calcium influx rather unlikely (Fig. S3). In many cases, delayed CaTs also were detected in the dendrite (Fig. S3). However, dendritic CaTs were delayed with respect to spine CaTs (2.8 ms, on average) and had smaller amplitudes (52% of spine CaTs, on average), which points to active calcium release inside the spine rather than passive diffusion of calcium from the dendrite into the spine.

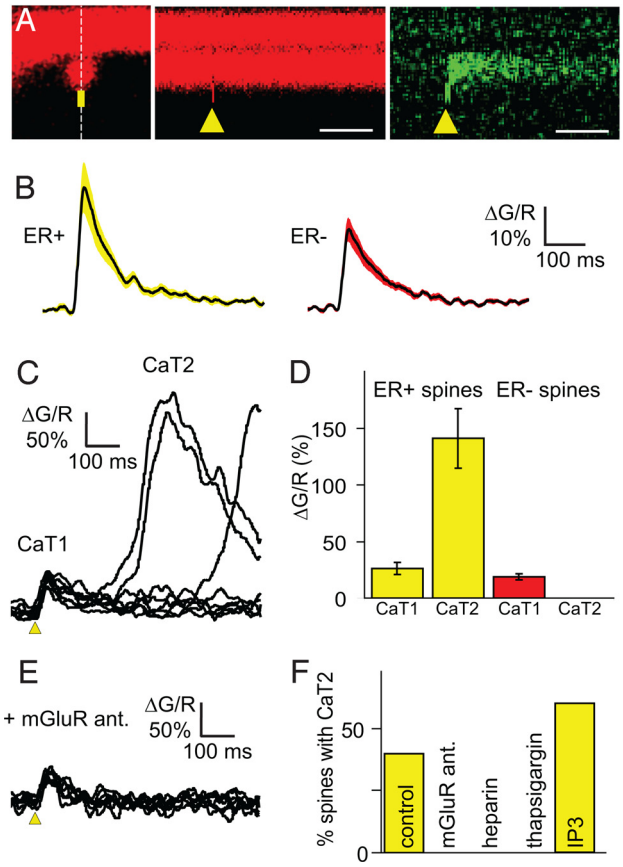

Fig. 3. Uncaging-evoked spine calcium transients. (*A*) Individual spines were stimulated by two-photon glutamate uncaging (yellow bar, arrowheads). Fluorescence of the calcium-sensitive dye (Fluo5F, green) was monitored in line scan mode and normalized by the fluorescence of the calcium-insensitive dye (Alexa Fluor 594, red). (Scale bars: 200 ms.) (*B*) Average time course of NMDAR-mediated calcium transients in ER-containing ($n = 19$) and other spines ($n = 26$). Colored region represents SEM. (*C*) Delayed calcium transients (CaT2) in an ER-containing spine (eight consecutive stimulations). (*D*) In ER+ spines (yellow), amplitudes of delayed calcium transients (CaT2) were large compared with NMDAR-mediated transients (CaT1) ($n = 19$). No CaT2 were observed in ER− spines ($n = 26$). Values represent mean ± SEM. (*E*) Group I mGluR block abolished delayed calcium transients (ER+ spine). (*F*) Pharmacological profile of delayed calcium transients in ER+ spines ($n = 19$, 9, 12, 9, and 5).

Blocking group I mGluRs with a mixture of mGluR1 and mGluR5 antagonists (100 μM LY367385 and 10 μM 2-Methyl-6-(phenylethynyl)pyridine hydrochloride (MPEP), $n = 9$) or blocking IP_3 receptors with intracellular heparin (4 mg/mL, $n = 12$) abolished delayed CaTs in ER+ spines (Fig. 3 *E* and *F*). Depletion of intracellular stores by bath application of thapsigargin also abolished delayed CaTs in ER+ spines (10 μM, $n = 9$). Whole-cell perfusion with 100 μM IP_3, however, increased the fraction of ER+ spines showing delayed CaTs ($n = 5$; Fig. 3*F*). The amplitude of uEPSCs was not affected by any of these pharmacological manipulations (Fig. S4). In summary, our data suggest that ER+ spines represent a specialized subpopulation of dendritic spines, capable of mGluR- and IP_3-mediated calcium signaling.

Group I mGluR receptors are preferentially located at the periphery of the synapse, and glutamate uncaging could activate a larger fraction of these perisynaptic receptors than vesicular glutamate release (22). To address this issue, we performed spine calcium imaging after electrical stimulation of Schaffer collaterals in acute slices (Fig. S5). With synaptic stimulation, four of 26 stimulated spines displayed delayed CaTs. Corre-

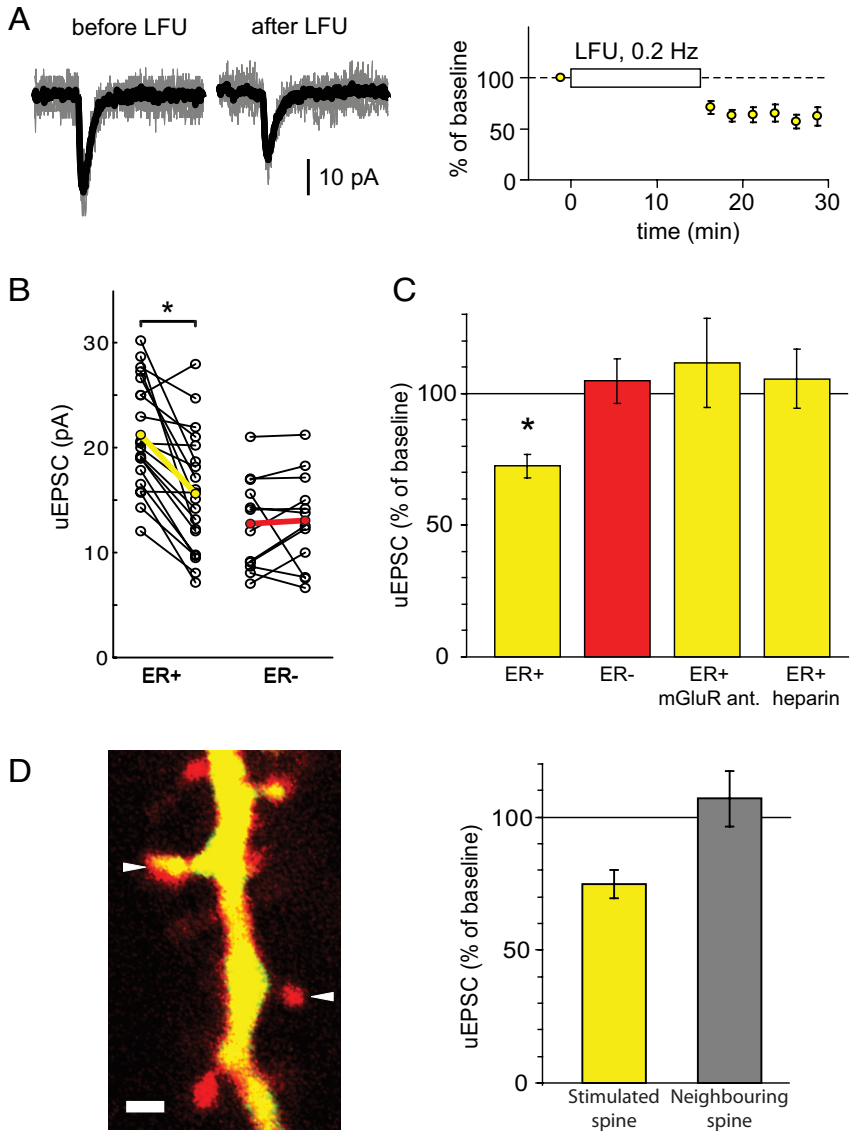

Fig. 4. Optical induction of synaptic depression. (*A*) uEPSCs before and after 15 min of glutamate LFU (0.2 Hz) on ER+ spine. Thick trace: Average of five uEPSCs. The LFU-induced depression was long-lasting (n = 6 ER+ spines; each time point represents the average response to five test pulses at 0.03 Hz). (*B*) The LFU-induced depression in ER-containing spines (n = 20, yellow circles mark the average uEPSC amplitude elicited by five test pulses before and immediately after 15 min of LFU), but not in other spines (n = 11, red circles mark mean uEPSCs). (*C*) Pharmacological profile of LFU-induced depression (metabotropic glutamate receptor antagonists, n = 7; heparin, n = 9). (*D*) The LFU-induced depression is homosynaptic (n = 8 spine pairs). Values in *A*, *C*, and *D* represent mean ± SEM.

sponding to the pharmacology of the uncaging experiments, thapsigargin (2 μM) completely prevented delayed CaTs after synaptic stimulation (0 of 33 spines). We conclude that at a subset of Schaffer collateral synapses delayed CaTs can be triggered by vesicular glutamate release from presynaptic terminals.

mGluR-Dependent Depression Is Restricted to ER-Containing Spines. With electrophysiological approaches, metabotropic signaling and IP_3-mediated calcium release have been suggested to be involved in the induction of LTD in several cortical areas (23–25). However, whether this form of plasticity is present at all synapses or restricted to a specialized subpopulation is unclear. mGluR-dependent LTD has been shown to have a strong postsynaptic component (26). The specificity of mGluR- → IP_3-mediated spine calcium signals raised the possibility that synapses on ER+ spines are preferential sites for this form of synaptic depression. We tested this possibility by comparing the effects of low-frequency stimulation, a classical LTD induction protocol, on ER+ spines. To isolate mGluR-dependent effects, NMDARs were blocked with dCPP (10 μM). In a series of control experiments, we verified that delayed CaTs were still present under NMDAR block (n = 4). The potency of synapses on spines of interest was measured before and after low-frequency uncaging (LFU) stimulation (0.2 Hz, 15 min; Fig. 4*A*). Indeed, low-frequency glutamate uncaging induced depression of the uEPSC in ER+ spines (72.4 ± 4.4% of baseline, n = 20; Fig. 4 *B* and *C*). This depression was long-lasting (n = 6; Fig. 4*A*) and stable (no significant difference between uEPSC amplitudes 15–17 and 27–30 min after start of LFU). Importantly, the same LFU protocol evoked no depression in spines lacking ER (104.7 ± 8.3% of baseline, n = 12; Fig. 4 *B* and *C*). Whole-cell perfusion with 1,2-bis(2-aminophenoxy)ethane-*N,N,N′,N′*-tetraacetate (BAPTA) (1 mM) blocked depression of uEPSC on ER+ spines (113.0 ± 5.1% of baseline, n = 3), indicating a calcium-dependent mechanism underlying depression. To test whether depression of uEPSCs at ER+ spines depended on

mGluR-mediated signaling, we pharmacologically blocked group I mGluRs (100 μM LY367385 and 10 μM MPEP) and analyzed the effects of the LFU protocol on synaptic potency. Blocking mGluRs did not affect the baseline response amplitude of ER+ spines (ER+, control, 21.0 ± 1.0 pA, n = 20; ER+, mGluR block, 21.3 ± 1.9, n = 7) but completely prevented LFU-induced depression (111.5 ± 16.9% of baseline, n = 7; Fig. 4*C*). We conclude that an mGluR-dependent mechanism was responsible for the difference in plasticity between ER+ and ER− spines. Depression at ER+ spines also was blocked completely by intracellular application of the IP_3 receptor antagonist heparin (105.5 ± 11.2% of baseline, n = 9; Fig. 4*C*). The identical pharmacology of synaptic depression, delayed CaTs, and the specificity for ER+ spines suggest that calcium release from the subsynaptic ER is required for the induction of NMDAR-independent depression at these synapses. Last, we investigated potential spread of synaptic depression by probing pairs of neighboring synapses on the same dendrite. As previously, LFU on ER+ spines produced reliable homosynaptic depression (74.7 ± 5.3% of baseline, n = 8). Remarkably, no significant change was detected at spine synapses 2–10 μm away (106.9 ± 10.5% of baseline; Fig. 4*E*), demonstrating that mGluR-dependent depression remains highly compartmentalized to individual synapses.

Discussion

A seemingly homogenous synaptic population, the Schaffer collateral projection onto CA1 pyramidal cells, displayed an astonishing diversity when we started to probe plasticity on the level of individual synapses. Repetitive activation of individual synapses triggered mGluR-mediated depression if and only if ER was present in close proximity to the synapse. Thus, this intracellular organelle appears to be capable of modulating spine calcium transients and synaptic plasticity on a local scale.

ER Is Associated with Mature Spines. We found spine ER not randomly distributed but specifically localized to large spines containing high-potency synapses (Fig. 2). Consistent with previous reports, synaptic potency was correlated with the volume of the spine head (15). Because newly formed spines are typically small (27), our data suggest that the acquisition of ER is part of the process of spine maturation. Overexpression of the adapter proteins Shank and Homer has been shown to enhance or accelerate this maturation process, leading to spine enlargement and recruitment of ER and IP_3 receptors into spines (28, 29). The preferential localization of ER to mature spines restricts the potential for mGluR- or IP_3-mediated calcium signaling to this specialized subpopulation. In this context, that the intact animal spines that are stable over days and weeks often contain ER is interesting (30). Altered sensory experience, for example, sensory deprivation, can lead to destabilization and removal of these stable spines (31). The mechanism that we describe here might be critical for the weakening and eventual disappearance of initially stable synaptic connections (27). Although only ≈20% of spines posses ER, they carry the synapses that contribute most excitatory drive and presumably need to be most tightly controlled (Fig. 2*C*).

mGluR Activation and Synaptic Plasticity. Ionotropic glutamate receptors, most prominently NMDARs, have been established to regulate the amplitude of spine calcium transients, an important trigger for synaptic plasticity (18, 32). The role of metabotropic receptors in regulating biochemical signaling in pyramidal neurons is less well understood. Strong activation of multiple presynaptic fibers can lead to the generation of mGluR-dependent calcium release events in apical dendrites (33). Here, we show that the activation of a single synapse can be sufficient to trigger mGluR-dependent calcium transients and depression if the activated synapse impinges on an ER+ spine (Fig. 3*F*). A similar metabotropic mechanism of depression has been described in Purkinje cells of the cerebellum (34, 35). In these cells, however, there is no indication of a regulation of plasticity on the single synapse level, a functional uniformity that is reflected in the homogenous morphology of Purkinje cell spines (36). Furthermore, much stronger stimulation is needed to elicit calcium release events in Purkinje cells, possibly related to the simpler, tube-like morphology of spine ER in these cells. Therefore, although the general mechanism of mGluR-mediated depression seems to be conserved in different cell types and brain areas, the selective targeting of the ER to strong synapses and the low activation threshold might be specific features of hippocampal pyramidal cells.

Our experiments suggest that local IP_3 receptor activation and calcium release are essential steps in the pathway leading from mGluRs to synaptic depression. Calcium release events and mGluR-dependent depression had identical pharmacological profiles: Both were blocked by group I mGluR antagonists and the IP_3 receptor blocker heparin. Furthermore, both processes were restricted to ER+ spines (Figs. 3*F* and 4*C*). This tight correlation and the sensitivity of depression to the calcium chelator BAPTA suggest that calcium release from the ER is a key step in the induction of synaptic depression. In our experiments, calcium release events were not restricted to the spine but often spread into the dendrite (Fig. S3). Induction of depression, however, was limited strictly to directly stimulated synapses (Fig. 4*D*). This specificity could be simply caused by differences in calcium signal amplitudes, but the ER also might serve additional functions during plasticity induction: In addition to regulating spine calcium signals, we show that it forms a continuous subcellular conduit for the exchange of proteins between dendrite and spine (Fig. 1*D*). Furthermore, ER-bound ribosomes provide a substrate for local mRNA translation, a process that is thought to be important for mGluR-mediated depression (37). The impact of ER on synaptic plasticity very likely involves all of the processes mentioned above. In summary, we show that differences in spine microanatomy, which were noted half a century ago (38), play a crucial functional role in determining the competence of individual synapses for long-term plasticity.

Materials and Methods

Slice Preparation and Plasmid Construction. Organotypic hippocampal slices were prepared from Wistar rats at postnatal day 5 as described (39). After 3–5 days in vitro, cultures were transfected with synapsin-GFP-ER and synapsin-RFP (tdimer2; R. Y. Tsien, University of California, San Diego), using a Helios gene gun (Bio-Rad). GFP-ER was constructed by fusing EGFP to the ER-targeting sequence of calreticulin and the ER-retention sequence KDEL.

Two-Photon Imaging and Uncaging. Imaging experiments were performed between 1 and 2 weeks after transfection. We used a custom-built two-photon imaging and uncaging setup (40) controlled by ScanImage (41). Two ultrafast IR lasers were combined for two-photon imaging (930 nm for GFP/RFP imaging, 810 nm for Alexa Fluor 594/Fluo5F imaging) and uncaging of 4-Methoxy-7-nitroindolinyl-caged L-glutamate (725 nm). To measure calcium signals, green and red fluorescence was collected during 250-Hz line scans across the spine head and parent dendrite (7–15 trials per spine). Fluorescence changes were quantified as increases in green fluorescence from baseline normalized to the red fluorescence ($\Delta G/R$) (42). For each imaging trial, photomultiplier dark noise was measured before shutter opening and subtracted from the dataset. Fluorescence was monitored 640 ms before the stimulus and 640 ms after the stimulus.

Glutamate uncaging was achieved by using a 0.5-ms laser pulse for experiments analyzing synaptic properties and a 1-ms pulse for experiments looking at synaptic depression. Mushroom-shaped spines well separated from neighboring spines were used for the experiments. The standard uncaging location was ≈0.5 μm from the spine center, in the direction away from the parent dendrite. These uncaging parameters minimized the possibility of activation of dendritic glutamate receptors. Laser intensity was ≈50 mW for 0.5-ms

NEUROSCIENCE

pulses and ≈40 mW for 1.0-ms pulses, measured in the back focal plane of the objective. The same laser pulse, if directed to the center of the spine, bleached 30% of the Alexa Fluor 594 fluorescence. We used this control to ensure equal stimulation strength for ER+ and ER− spines (14) (Fig. S2).

Electrophysiology. Slice cultures were superfused with artificial cerebrospinal fluid (ACSF) at 30–32 °C containing 127 mM NaCl, 25 mM $NaHCO_3$, 25 mM D-glucose, 2.5 mM KCl, 1 mM $MgCl_2$, 2 mM $CaCl_2$, 1.25 mM NaH_2PO_4, 0.05 mM chloroadenosine, and 0.01 mM serine. For uncaging experiments, 5 mM MNI-glutamate (Tocris) was added to the ACSF. For plasticity experiments, serine was replaced by 0.01 mM dCPP in the ACSF. To block mGluR1 and mGluR5 receptors, we added LY367385 (0.1 mM; Tocris) and MPEP (0.01 mM, kindly provided by Novartis AG). To deplete internal calcium stores we used thapsigargin (0.01). Whole-cell recordings were made with an Axopatch 200B amplifier (Axon Instruments), using 4–6 MΩ electrodes filled with 135 mM potassium gluconate, 10 mM Hepes, 10 mM sodium phosphocreatine, 3 mM sodium ascorbate, 4 mM $MgCl_2$, 4 mM Na_2-ATP, 0.4 mM Na-GTP, and 0.015 mM Alexa Fluor 594 (pH 7.2). For calcium imaging experiments, 0.3 mM Fluo5F (Molecular Probes) was added. Calcium imaging experiments were performed under current clamp conditions, and measurements of postsynaptic currents were performed in voltage clamp. The uEPSC peak amplitude was extracted by fitting the difference of two exponentials to the average electrical response for each spine (five trials per spine). To allow for dye and drug diffusion, we started the stimulation 15–20 min after break-in.

Induction of Synaptic Depression at Single Spines. We attempted to mimic a conventional low-frequency LTD stimulation protocol (15 min, 1 Hz, 900 pulses). Because, in contrast to the reliable uncaging stimulus, the average release probability of Schaffer collateral synapses is only ≈0.2, we used a five times lower frequency for the LFU stimulation (15 min, 0.2 Hz, 180 pulses). To optimize the signal-to-noise ratio of the electrical recording, only spines with an average uEPSC >7 pA were selected for the experiment. To quantify synaptic response amplitude, spines were stimulated before and after LFU with five test pulses spaced 30 s apart. To quantify depression, the average response after LFU was divided by the average response before LFU. For long-term recordings after LFU, spines were stimulated with test pulses at 0.03 Hz. Cells were held in voltage clamp at −65 mV.

Statistical Analysis. Data are reported as mean ± SEM. To test for significance we used the Mann–Whitney rank sum test (unpaired data) or the Wilcoxon signed-rank test (paired data) at a significance level of $P = 0.05$.

ACKNOWLEDGMENTS. We thank D. Gerosa-Erni for excellent technical support and R.W. Friedrich, C.E. Gee, A. Lüthi, and A. Matus for critical discussions and reading the manuscript. The work was supported by the Novartis Research Foundation, SystemsX.ch, and the Gebert Rüf Foundation.

1. Bliss TV, Collingridge GL (1993) A synaptic model of memory: Long-term potentiation in the hippocampus. *Nature* 361:31–39.
2. Oliet SH, Malenka RC, Nicoll RA (1997) Two distinct forms of long-term depression coexist in CA1 hippocampal pyramidal cells. *Neuron* 18:969–982.
3. Liu L, et al. (2004) Role of NMDA receptor subtypes in governing the direction of hippocampal synaptic plasticity. *Science* 304:1021–1024.
4. Bear MF, Huber KM, Warren ST (2004) The mGluR theory of fragile X mental retardation. *Trends Neurosci* 27:370–377.
5. Bellone C, Luscher C, Mameli M (2008) Mechanisms of synaptic depression triggered by metabotropic glutamate receptors. *Cell Mol Life Sci* 65:2913–2923.
6. Cooney JR, Hurlburt JL, Selig DK, Harris KM, Fiala JC (2002) Endosomal compartments serve multiple hippocampal dendritic spines from a widespread rather than a local store of recycling membrane. *J Neurosci* 22:2215–2224.
7. Deller T, et al. (2003) Synaptopodin-deficient mice lack a spine apparatus and show deficits in synaptic plasticity. *Proc Natl Acad Sci USA* 100:10494–10499.
8. Vlachos A, et al. (2009) Synaptopodin regulates plasticity of dendritic spines in hippocampal neurons. *J Neurosci* 29:1017–1033.
9. Toresson H, Grant SG (2005) Dynamic distribution of endoplasmic reticulum in hippocampal neuron dendritic spines. *Eur J Neurosci* 22:1793–1798.
10. Svoboda K, Tank DW, Denk W (1996) Direct measurement of coupling between dendritic spines and shafts. *Science* 272:716–719.
11. Bloodgood BL, Sabatini BL (2005) Neuronal activity regulates diffusion across the neck of dendritic spines. *Science* 310:866–869.
12. Biess A, Korkotian E, Holcman D (2007) Diffusion in a dendritic spine: The role of geometry. *Phys Rev E Stat Nonlin Soft Matter Phys* 76:021922.
13. Deller T, Merten T, Roth SU, Mundel P, Frotscher M (2000) Actin-associated protein synaptopodin in the rat hippocampal formation: Localization in the spine neck and close association with the spine apparatus of principal neurons. *J Comp Neurol* 418:164–181.
14. Bloodgood BL, Sabatini BL (2007) Nonlinear regulation of unitary synaptic signals by $CaV_{2.3}$ voltage-sensitive calcium channels located in dendritic spines. *Neuron* 53:249–260.
15. Matsuzaki M, et al. (2001) Dendritic spine geometry is critical for AMPA receptor expression in hippocampal CA1 pyramidal neurons. *Nat Neurosci* 4:1086–1092.
16. Harvey CD, Svoboda K (2007) Locally dynamic synaptic learning rules in pyramidal neuron dendrites. *Nature* 450:1195–1200.
17. Brocher S, Artola A, Singer W (1992) Intracellular injection of Ca^{2+} chelators blocks induction of long-term depression in rat visual cortex. *Proc Natl Acad Sci USA* 89:123–127.
18. Nevian T, Sakmann B (2006) Spine Ca^{2+} signaling in spike-timing-dependent plasticity. *J Neurosci* 26:11001–11013.
19. Bloodgood BL, Sabatini BL (2007) Ca^{2+} signaling in dendritic spines. *Curr Opin Neurobiol* 17:345–351.
20. Sobczyk A, Svoboda K (2007) Activity-dependent plasticity of the NMDA-receptor fractional Ca^{2+} current. *Neuron* 53:17–24.
21. Grunditz A, Holbro N, Tian L, Zuo Y, Oertner TG (2008) Spine neck plasticity controls postsynaptic calcium signals through electrical compartmentalization. *J Neurosci* 28:13457–13466.
22. Lujan R, Roberts JD, Shigemoto R, Ohishi H, Somogyi P (1997) Differential plasma membrane distribution of metabotropic glutamate receptors mGluR1α, mGluR2 and mGluR5, relative to neurotransmitter release sites. *J Chem Neuroanat* 13:219–241.
23. Reyes M, Stanton PK (1996) Induction of hippocampal long-term depression requires release of Ca^{2+} from separate presynaptic and postsynaptic intracellular stores. *J Neurosci* 16:5951–5960.
24. Nishiyama M, Hong K, Mikoshiba K, Poo MM, Kato K (2000) Calcium stores regulate the polarity and input specificity of synaptic modification. *Nature* 408:584–588.
25. Bender VA, Bender KJ, Brasier DJ, Feldman DE (2006) Two coincidence detectors for spike timing-dependent plasticity in somatosensory cortex. *J Neurosci* 26:4166–4177.
26. Zhang XL, Zhou ZY, Winterer J, Muller W, Stanton PK (2006) NMDA-dependent, but not group I metabotropic glutamate receptor-dependent, long-term depression at Schaffer collateral–CA1 synapses is associated with long-term reduction of release from the rapidly recycling presynaptic vesicle pool. *J Neurosci* 26:10270–10280.
27. Yasumatsu N, Matsuzaki M, Miyazaki T, Noguchi J, Kasai H (2008) Principles of long-term dynamics of dendritic spines. *J Neurosci* 28:13592–13608.
28. Sala C, Roussignol G, Meldolesi J, Fagni L (2005) Key role of the postsynaptic density scaffold proteins Shank and Homer in the functional architecture of Ca^{2+} homeostasis at dendritic spines in hippocampal neurons. *J Neurosci* 25:4587–4592.
29. Sala C, et al. (2001) Regulation of dendritic spine morphology and synaptic function by Shank and Homer. *Neuron* 31:115–130.
30. Knott GW, Holtmaat A, Wilbrecht L, Welker E, Svoboda K (2006) Spine growth precedes synapse formation in the adult neocortex in vivo. *Nat Neurosci* 9:1117–1124.
31. Holtmaat A, Wilbrecht L, Knott GW, Welker E, Svoboda K (2006) Experience-dependent and cell-type-specific spine growth in the neocortex. *Nature* 441:979–983.
32. MacDonald JF, Jackson MF, Beazely MA (2006) Hippocampal long-term synaptic plasticity and signal amplification of NMDA receptors. *Crit Rev Neurobiol* 18:71–84.
33. Nakamura T, Barbara JG, Nakamura K, Ross WN (1999) Synergistic release of Ca^{2+} from IP_3-sensitive stores evoked by synaptic activation of mGluRs paired with backpropagating action potentials. *Neuron* 24:727–737.
34. Finch EA, Augustine GJ (1998) Local calcium signalling by inositol-1,4,5-trisphosphate in Purkinje cell dendrites. *Nature* 396:753–756.
35. Miyata M, et al. (2000) Local calcium release in dendritic spines required for long-term synaptic depression. *Neuron* 28:233–244.
36. Harris KM, Stevens JK (1988) Dendritic spines of rat cerebellar Purkinje cells: Serial electron microscopy with reference to their biophysical characteristics. *J Neurosci* 8:4455–4469.
37. Huber KM, Kayser MS, Bear MF (2000) Role for rapid dendritic protein synthesis in hippocampal mGluR-dependent long-term depression. *Science* 288:1254–1257.
38. Gray EG (1959) Electron microscopy of synaptic contacts on dendrite spines of the cerebral cortex. *Nature* 183:1592–1593.
39. Stoppini L, Buchs PA, Muller D (1991) A simple method for organotypic cultures of nervous tissue. *J Neurosci Methods* 37:173–182.
40. Zhang YP, Holbro N, Oertner TG (2008) Optical induction of plasticity at single synapses reveals input-specific accumulation of αCaMKII. *Proc Natl Acad Sci USA* 105:12039–12044.
41. Pologruto TA, Sabatini BL, Svoboda K (2003) ScanImage: Flexible software for operating laser scanning microscopes. *Biomed Eng Online* 2:13.
42. Yasuda R, et al. (2004) Imaging calcium concentration dynamics in small neuronal compartments. *Sci STKE*, pl5.